

DRAGONFLY IMAGING OF THE GALAXY NGC 5907: A REVISED VIEW OF THE ICONIC STELLAR STREAM

PIETER VAN DOKKUM¹, COLLEEN GILHULY², ANA BONACA³, ALLISON MERRITT⁴, SHANY DANIELI^{1,5}, DEBORAH LOKHORST²,
ROBERTO ABRAHAM², CHARLIE CONROY³, JOHNNY P. GRECO⁶

Submitted to ApJ Letters

ABSTRACT

In 2008 it was reported that the stellar stream of the edge-on spiral NGC 5907 loops twice around the galaxy, enveloping it in a giant corkscrew-like structure. Here we present imaging of this iconic object with the Dragonfly Telephoto Array, reaching 1σ surface brightness levels of $\mu_g \approx 30.5$ mag arcsec⁻² on arcminute scales. We find that the stream has a qualitatively different morphology from that reported in the 2008 study. The Dragonfly data do not show two loops but a single curved stream with a total length of 45' (220 kpc). The surface brightness of the stream ranges from $\mu_g \approx 27.6$ mag arcsec⁻² to $\mu_g \approx 28.8$ mag arcsec⁻², and it extends significantly beyond the region where tidal features had previously been detected. We find a density enhancement near the luminosity-weighted midpoint of the stream which we identify as the likely remnant of a nearly-disrupted progenitor galaxy. A restricted N-body simulation provides a qualitative match to all detected features with little fine-tuning. In terms of its spatial extent and stellar mass the stream is similar to Sagittarius, and our results demonstrate the efficacy of low surface brightness-optimized telescopes for obtaining maps of such large streams outside the Local Group. The census of these rare, relatively high mass events complements the census of common, low mass ones that is provided by studies of streams in the Milky Way halo.

1. INTRODUCTION

Stellar streams, the debris of tidally-disrupted globular clusters or galaxies, provide information on the frequency of the accretion of small objects onto larger ones (see, e.g., Bullock & Johnston 2005). As their morphologies reflect their orbits they are also probes of the gravitational potential, and they have been used as a tool to constrain the mass and structure of dark matter halos (Moore et al. 1999; Ibata et al. 2002; Helmi 2004; Law & Majewski 2010; Bovy, Erkal, & Sanders 2017; Bonaca & Hogg 2018).

In the Milky Way more than 40 stellar streams have been identified (see Grillmair & Carlin 2016; Shipp et al. 2018), with Sagittarius (Ibata et al. 1997), Palomar 5 (Odenkirchen et al. 2001), Monoceros (Newberg et al. 2002), and the “orphan stream” (Belokurov et al. 2007) among the most prominent examples. This number is increasing rapidly, thanks to the increased contrast attainable with Gaia and deep star count maps (see, e.g., Malhan, Ibata, & Martin 2018; Bonaca et al. 2019). Likewise, M31 is home to many tidally-disrupting satellite objects, ranging from low mass “stretched” objects such as Andromeda XIX (McConnachie et al. 2008) to the major event, or events, that were responsible for shaping the complex structure of the M31 halo (Ibata et al. 2001; Hammer et al. 2010).

At distances $D \gtrsim 5$ Mpc streams can be identified by the smooth integrated light of their stellar populations (e.g., Arp

1966; Malin & Hadley 1997; Forbes et al. 2003; Mihos et al. 2005; van Dokkum 2005; Bell et al. 2006; Martínez-Delgado et al. 2010; Atkinson, Abraham, & Ferguson 2013). Such integrated-light measurements typically do not reach the same stellar density limits as star count surveys but probe a much greater volume of the Universe (see Danieli, van Dokkum, & Conroy 2018, for a quantitative discussion). The combination of studies of frequent, low mass accretion events in the Local Group with systematic integrated-light surveys of rare, high mass events around other galaxies should ultimately provide a complete census of present-day accretion-driven galaxy growth.

One of the best-known tidal features outside of the Local Group is the stellar stream associated with NGC 5907, an edge-on spiral galaxy with a stellar mass of $\approx 8 \times 10^{10} M_\odot$ (Laine et al. 2016) at a distance of 17 Mpc (Tully, Courtois, & Sorce 2016). The stream was discovered by Shang et al. (1998) and Zheng et al. (1999), who detected sections of a loop around the disk of NGC 5907 using the Beijing Astronomical Observatory 0.6/0.9 m Schmidt telescope. This was a remarkable discovery, as previous deep optical and HI searches had not uncovered any tidal features associated with NGC 5907 (see Sancisi 1976; Sasaki 1987; Sackett et al. 1994). The galaxy was subsequently imaged by Martínez-Delgado et al. (2008) [hereafter M08], using a 0.5 m Ritchey-Chrétien telescope. M08 report that the stream exhibits not one but two complete loops, enveloping NGC 5907 in a giant corkscrew-like structure. Their evocative image has taken on an iconic status, serving as a powerful demonstration of the shredding of a small galaxy.⁷ Some years later NGC 5907 was also observed by Laine et al. (2016), who combined mid-IR data from the IRAC camera on the Spitzer Space Telescope with optical 8 m Subaru telescope images. These authors studied the part of the stream that was detected by Shang et al. (1998) and do not comment on the second loop that was

¹ Astronomy Department, Yale University, 52 Hillhouse Ave, New Haven, CT 06511, USA

² Department of Astronomy & Astrophysics, University of Toronto, 50 St. George Street, Toronto, ON M5S 3H4, Canada

³ Harvard-Smithsonian Center for Astrophysics, 60 Garden Street, Cambridge, MA, USA

⁴ Max-Planck-Institut für Astronomie, Königstuhl 17, D-69117 Heidelberg, Germany

⁵ Physics Department, Yale University, 52 Hillhouse Ave, New Haven, CT 06511, USA

⁶ Center for Cosmology and AstroParticle Physics (CCAPP), The Ohio State University, Columbus, OH 43210, USA

⁷ We note that Wang et al. (2012) interpret the M08 data as evidence of a major merger.

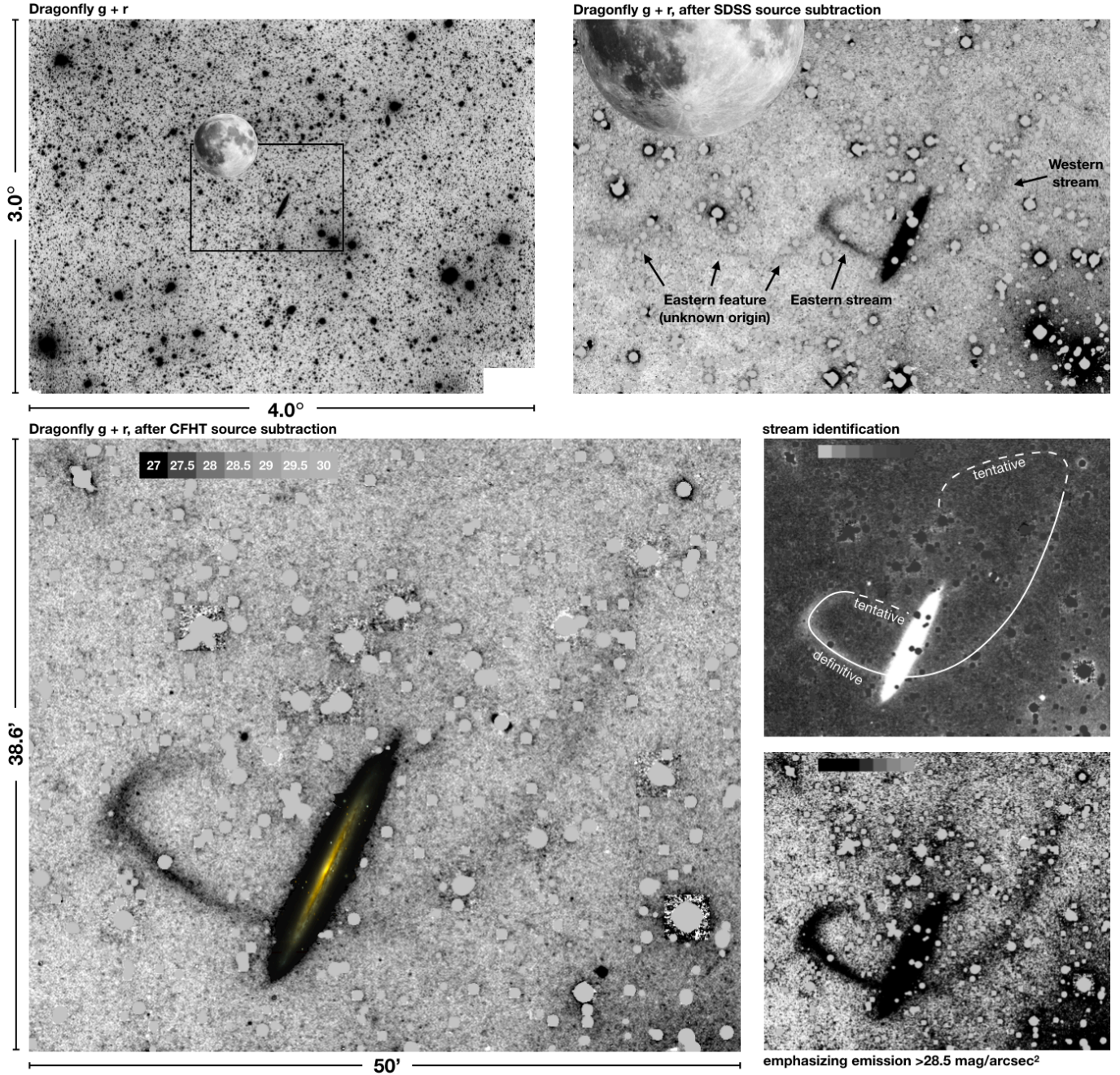


Figure 1. Dragonfly imaging of the NGC 5907 field, with North up and East to the left. *Top left:* sum of the g and r band images, with the moon shown for scale. The effective exposure time is 4.8 hr. *Top right:* zoom on the vicinity of NGC 5907, after subtracting a model of compact emission in the frame. The model is based on SDSS g and r band images. The image shows a single coherent stellar stream with a length of $\approx 45'$ that crosses the galaxy. We also identify a thin, linear feature to the East and a low surface brightness patch 1° from NGC 5907. *Bottom panels:* the region of the NGC 5907 stream, at three different scalings. The compact emission model in this region is based on deep CFHT imaging. The scale bar at the top indicates the surface brightness in AB mag arcsec $^{-2}$. For reference a color image of NGC 5907, created from Beijing-Arizona All Sky Survey data, is also shown.

reported by M08.

Here we report on new low surface brightness imaging of NGC 5907 over a wide field, as part of an imaging campaign of nearby galaxies with the Dragonfly Telephoto Array (Abraham & van Dokkum 2014). We are conducting two surveys, the Dragonfly Nearby Galaxy Survey (Merritt et al. 2016) and the Dragonfly Edge-on Galaxy Survey (C. Gilhuly et al., in preparation); NGC 5907 was one of the first targets of the edge-on survey.

2. DATA

2.1. Observations and reduction

The observations were obtained with the Dragonfly Telephoto Array, a low surface brightness-optimized telescope consisting of 48 Canon 400 mm $f/2.8$ II telephoto lenses. Its basic design and its previous eight-lens configuration are described in Abraham & van Dokkum (2014), Merritt et al. (2016), and Zhang et al. (2018). The current 48-lens array is described in S. Danieli et al., in preparation. Briefly,

each lens is coupled to an SBIG STT-8300M camera offering a 2.6×1.9 instantaneous field of view with $2''.8$ native pixels and a FWHM spatial resolution of $\approx 6''.7$. The lenses are intentionally offset from one another by $\approx 10\%$ of the field of view, giving 48 independent sightlines. Data are taken with large ($\approx 25'$) dithers between exposures, providing further redundancy. As the data are sky-limited in our 600 s integrations the telescope behaves optically like a 1.0 m $f/0.4$ refractor with superb optical surfaces and near-perfect baffling. Twenty-four lenses are equipped with SDSS g filters and 24 with SDSS r filters.

The data reduction is gate-based, executing multiple quality tests on each frame as it progresses through the pipeline. Furthermore, the reduction pipeline has two stages. After the first stage a mask is generated containing all detected emission in the co-added image. This is used in the second stage to mask all emission sources from the individual raw frames prior to determining the background. The pipeline is described in detail in Jielai Zhang’s PhD thesis⁸ and in S. Danieli et al., in preparation. The total number of frames that went into the final NGC 5907 stacks is 618 in g and 762 in r ; this is the equivalent of 4.8 hr with the full 48 lens array. The summed $g+r$ image is shown in the top left of Fig. 1; owing to the dithering it covers 12 degree^2 , with reduced effective exposure time near the edges of the field.

2.2. Multi-resolution filtering

The Dragonfly data have excellent low surface brightness sensitivity and are essentially free of ghosts, reflections, and other artifacts. However, they suffer from crowding due to the relatively low spatial resolution. We subtracted compact emission sources from the data using multi-resolution filtering (MRF). Details are given in P. van Dokkum et al., in preparation. Briefly, a flux model is created by multiplying an image of higher resolution (such as archival CFHT data) by a SExtractor (Bertin & Arnouts 1996) object map of that image. Any detected low surface brightness features in the high resolution data can be removed from the model at this stage. The model is then convolved with a kernel to match the Dragonfly resolution and subtracted. Remaining halos around bright stars are removed following a similar process as described in van Dokkum, Abraham, & Merritt (2014).

The results are shown in Fig. 1. For the image at top right the high resolution model was created from SDSS g and r images. These are shallow but have few artifacts and enable a wide field subtraction. The images in the bottom panels were filtered using a combination of Canada France Hawaii Telescope (CFHT) and Beijing-Arizona All Sky Survey (BASS; Zou et al. 2018) imaging. The BASS data are only used to identify and remove artifacts and missing data in the CFHT images. The CFHT imaging comprises 2100 s in g and 1500 s in r . We carefully checked that no low surface brightness emission is contained in the high resolution model. The only low surface brightness object that we removed from the model is a previously-uncataloged dwarf galaxy.

3. OBSERVATIONAL RESULTS

3.1. Morphology and photometry of the stream

The Dragonfly images show a relatively straightforward stream morphology. We confirm the existence of the strongly

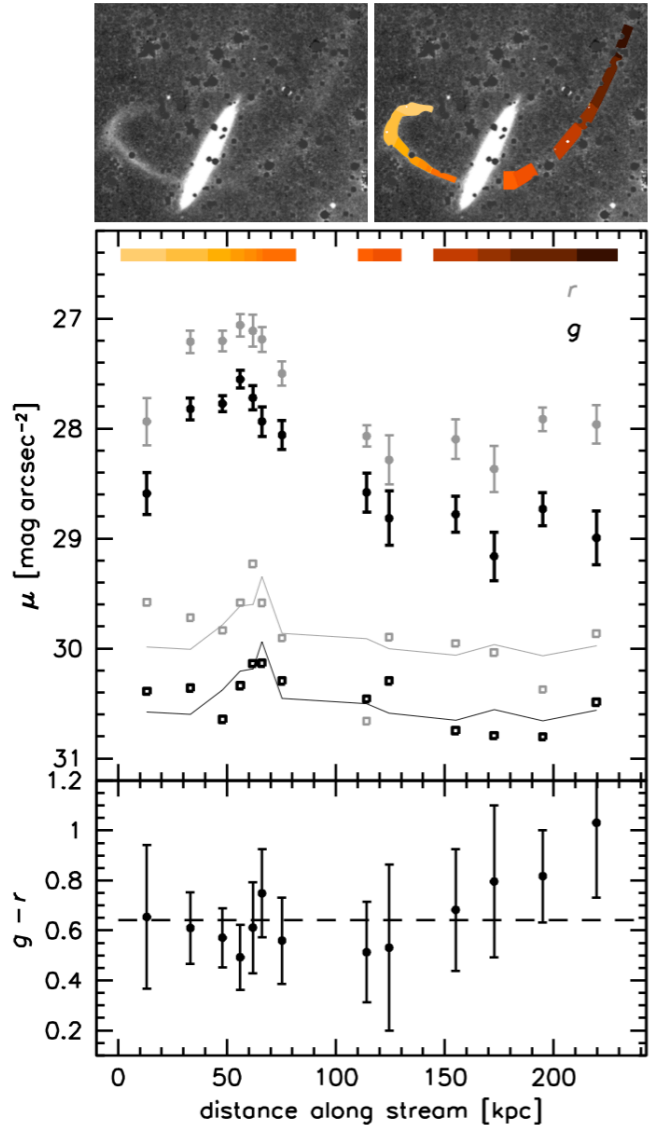


Figure 2. Photometry along the stream. *Top panel:* g - and r -band surface brightness. Open symbols indicate the 1σ uncertainty, derived by placing the stream apertures in empty regions of the image. This uncertainty is $\sigma(\mu_g) \approx 30.25 + 0.5 \log(A) \text{ mag arcsec}^{-2}$, with A the aperture size in arcmin² (thin line). The average surface brightness of the stream is $\mu_g \approx 27.8$ on the East side of the galaxy and $\mu_g \approx 28.8 \text{ mag arcsec}^{-2}$ on the West side. *Bottom panel:* Average $g-r$ color profile. The weighted mean color is $\langle g-r \rangle = 0.64$.

curved Eastern stream that was discovered by Shang et al. (1998) (see top right panel of Fig. 1). We find that the stream continues on the West side of NGC 5907 at lower surface brightness. This Western stream reaches more than twice the length of the Eastern stream. This stream morphology is qualitatively different from the double loop structure reported by M08; we return to this in § 5. We also detect a thin feature extending from the brightest part of the stream to the East and a faint patch about 1° due East of NGC 5907. These faint features are not artifacts and are seen in both g and r ; their nature is unclear. Finally, we tentatively detect continuations of the stream at both ends: there may be a thin extension of the Western stream toward the Northeast, looping back South toward the disk, and there is a likely continuation of the Eastern stream toward the disk. Both these extensions are labeled

⁸ https://jielaizhang.github.io/files/Zhang_Jielai_201811_PhD_Thesis_excludech4.pdf

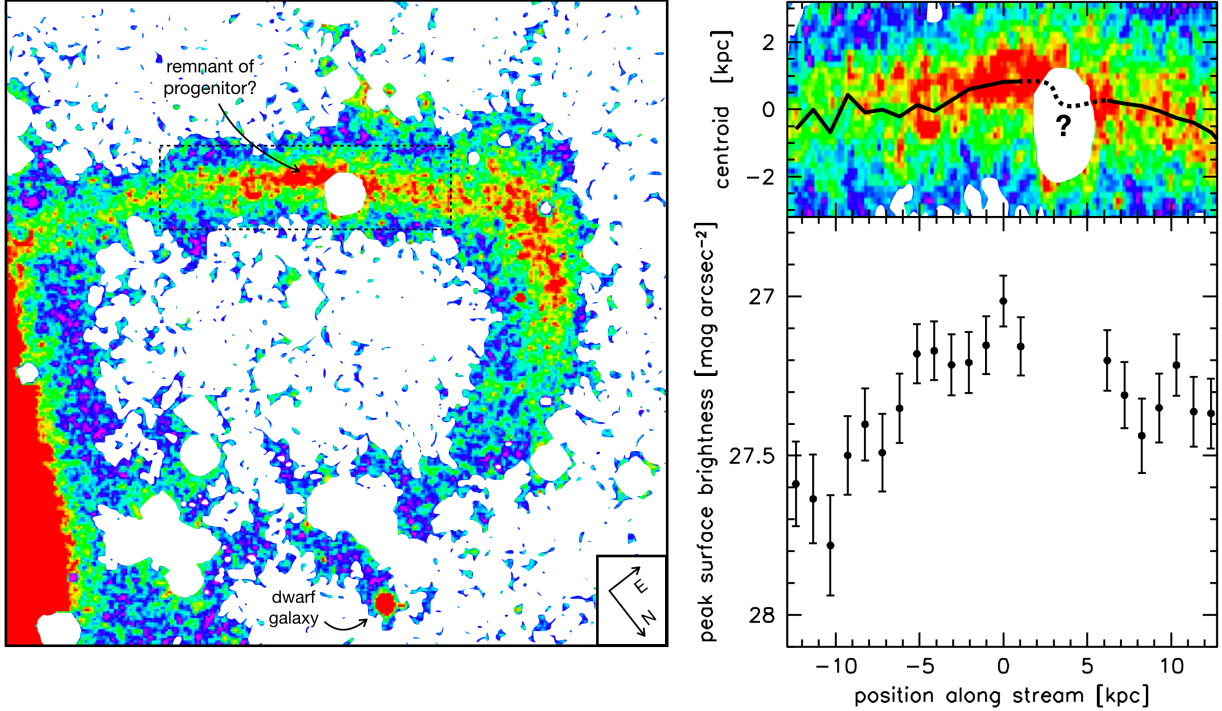


Figure 3. *Left:* False color image of the Eastern stream, rotated by 142° . *Right:* Results of Gaussian fits in $12''/5$ bins along the stream segment shown in the box at left. The top panel shows the best-fit position and the bottom panel shows the surface brightness of the peak of the Gaussian. There is a clear stellar density enhancement in this region, and a possible asymmetry. This area is close to the luminosity-weighted midpoint of the stream.

“tentative” in Fig. 1, and they are not included in our analysis.

The average surface brightness along the stream in g and r is quantified using aperture photometry. The apertures aim to include most of the width of the stream. As shown in Fig. 2 the average surface brightness reaches a peak of $\mu_g \approx 27.6$ mag arcsec $^{-2}$ on the East side of the galaxy. On the West side the surface brightness is lower at $\mu_g \approx 28.8$ mag arcsec $^{-2}$. Uncertainties are determined by moving each aperture off of the actual stream and then obtaining fluxes in these “empty” locations. By using 13 independent positions and mirroring the stream in x and y we obtain 52 empty aperture measurements. The 1σ variation in these measurements is taken as the uncertainty (open symbols in Fig. 2). The uncertainty is approximately $\sigma(\mu_g) \approx 30.25 + 0.5 \log(A)$ and $\sigma(\mu_r) \approx 29.66 + 0.5 \log(A)$, with A the aperture size in arcmin 2 (thin lines). The $g-r$ color along the stream is shown in the bottom panel. The data are consistent with a constant color along the stream of $\langle g-r \rangle \approx 0.64$ mag, although we cannot exclude color variation at the level of $0.1-0.2$ mag. The systematic error in the mean color is mainly driven by sky subtraction uncertainties on large scales ($\gtrsim 30'$), and estimated at ~ 0.1 mag. These results are broadly consistent with Shang et al. (1998) and Laine et al. (2016), who obtained photometry for the relatively bright Eastern part of the stream only.

The total magnitudes integrated over all apertures are $m_g = 15.5$ and $m_r = 14.8$. There are two gaps in the photometric apertures: one coinciding with the disk and another with a bright star (see top right panel of Fig. 2). Interpolating over these apertures suggests these regions contain $\approx 10\%$ of the light of the stream. Assuming another 10% is missed in regions that are fainter than our detection limit, we estimate that the total magnitudes of the stream are $m_g \approx 15.3$ and $m_r \approx 14.6$. For $D = 17$ Mpc this corresponds to $L_g \approx 1.8 \times 10^8 L_\odot$.

For an analysis of the stellar population of the stream we refer the reader to Laine et al. (2016).

3.2. Probable identification of the progenitor galaxy

Stellar streams are generated by mass loss from a progenitor object along its orbit, and in well-defined streams such as Sagittarius and Palomar 5 the disrupting progenitor is clearly identified (Ibata et al. 1997; Odenkirchen et al. 2001). Generally the progenitor object should be embedded within the densest part of the stream, should be near the luminosity-weighted midpoint of the stream, and should coincide with a displacement in the stream (as the leading and trailing streams come from stars that became unbound at opposite Lagrange points, toward the center and anti-center of the potential). These are not absolutes, as the orbital geometry, the superposition of successive passages, and projection effects complicate the observed morphology.

We identify the likely remnant of the progenitor object within the region highlighted with the box in the left panel of Fig. 3. In the right panel we show the centroid of the emission and the peak brightness as a function of the position along this stream segment. These values are determined by fitting Gaussians to the stream profile, averaging the $g+r$ emission in $12''/5$ sections along the stream. There is a clear, broad peak in the surface brightness, close to the luminosity-weighted midpoint of the stream: $\sim 40\%$ of the luminosity is to the East and $\sim 60\%$ to the West. Furthermore, the centroid shows several ~ 1 kpc-sized offsets that could indicate the characteristic displacement of the leading and trailing streams. A possible location is indicated by the broken line and the question mark; unfortunately it coincides with a bright foreground star.

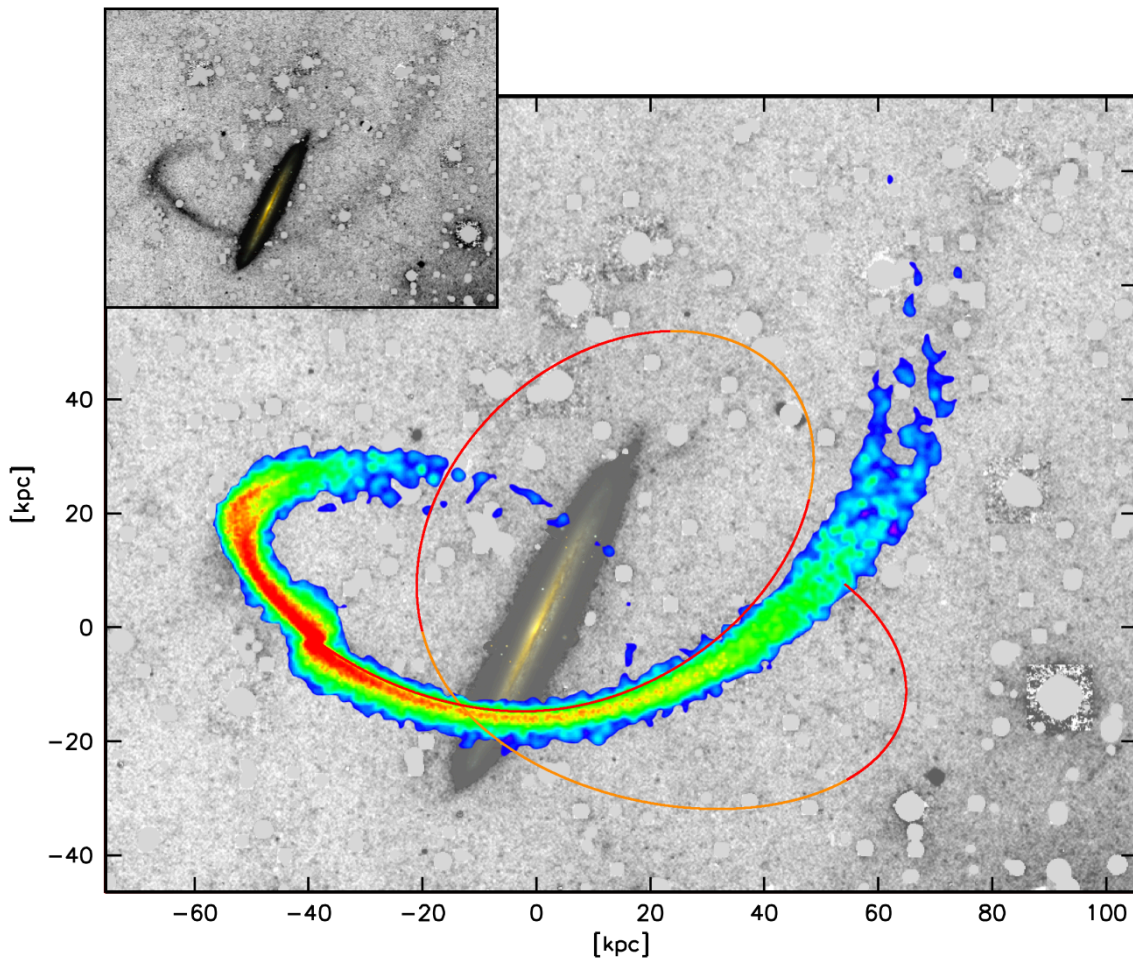


Figure 4. Restricted N-body simulation of a disrupting galaxy with a mass of $2 \times 10^8 M_{\odot}$, with its present-day location matched to that of the progenitor identified in § 3.2. The model reproduces the key observed aspects of the observed stream. The line indicates the most recent 2.5 Gyr of the orbit, with red and orange alternating every 0.5 Gyr.

In this section we show that a tidally disrupting satellite reproduces the overall stream morphology and the identified location of the progenitor. We followed the methodology developed for modeling streams in the Milky Way (e.g., Price-Whelan & Bonaca 2018), and started by rotating the coordinate system such that the galaxy is aligned with the x -axis, z is perpendicular to the disk plane and y is the radial direction. The gravitational potential is set up with the same assumptions as M08 used for the disk (mass: $2.3 \times 10^{10} M_{\odot}$, scale-length: 6.24 kpc, scale-height: 0.26 kpc), bulge (mass: $2.3 \times 10^{10} M_{\odot}$, scale-radius: 0.6 kpc), and halo (mass: $1.96 \times 10^{11} M_{\odot}$, scale-radius: 8.2 kpc). M08 used a spherical halo but we adopted an axis ratio $q_z = 0.95$, as this better reproduces the curvature of the trailing tail.

With the potential in place, we searched for the 6D location of the progenitor until we obtained an orbit that approximately matches the detected stream positions. The progenitor is assumed to be at the approximate x, z position determined in § 3.2, and for simplicity we set $y = 0$. The velocity is tweaked in the positive x, z direction, as the morphology suggests that the Eastern stream is the leading tail. In our model, the progenitor is currently at $\vec{x} = (-19.0, 0.0, 33.8)$ kpc, $\vec{v} = (30, 85, 165)$ km s $^{-1}$. Due to projection effects and the lack of kinematic data this solution is not unique, but we leave a full exploration of the parameter space to future work.

With the orbit determined, we created a mock stream using the Fardal, Huang, & Weinberg (2015) method implemented in the `gala` package (Price-Whelan 2017). During the most recent 2.5 Gyr of the orbit we released tracer particles from the progenitor, tuning the spatial and kinematic offsets of the escaping stars to best represent the shape of the observed stream close to the progenitor. The progenitor initially had a stellar mass of $2 \times 10^8 M_{\odot}$.

The orbit and mock stream are shown in Fig. 4. The colors are a density map, obtained by adaptively smoothing the particles. There are discrepancies on small scales: the displacement of the tails at the Lagrange points is larger than in the data, and the complex structure within the Northeastern loop is not reproduced. However, the model captures the key elements of the observed stream: it reproduces its overall path, the higher density of the leading (Eastern) tail, and the asymmetric broadening of the leading tail where it curves back toward NGC 5907.

5. DISCUSSION

In this *Letter* we present Dragonfly imaging of the NGC 5907 system, focusing on its well-known stellar stream. We find a relatively straightforward system composed of the remnant of a progenitor galaxy, a leading tail, and a long faint trailing tail. This overall morphology can be reproduced with

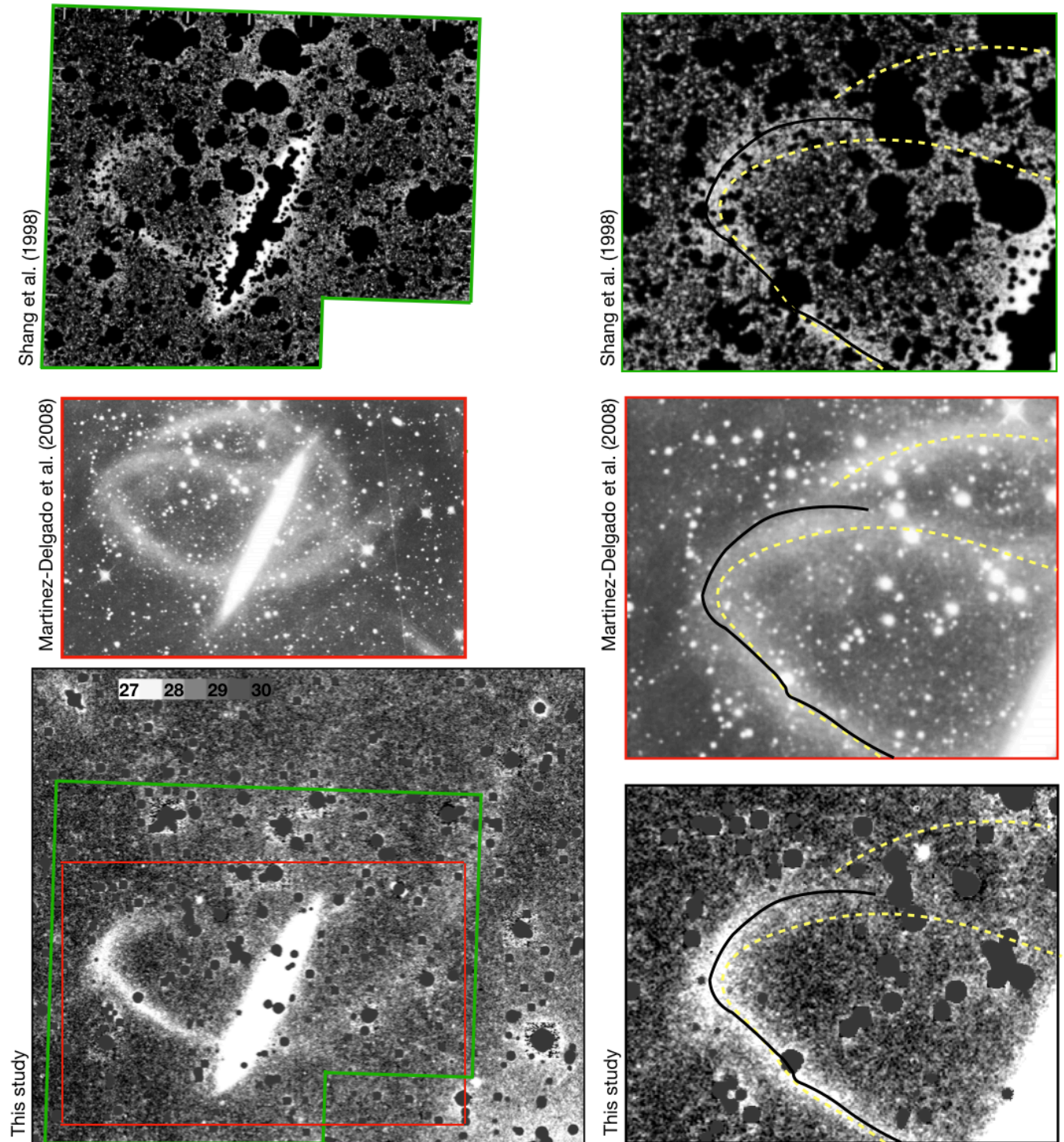


Figure 5. Comparison to the discovery image of Shang et al. (1998) and the follow-up study of Martínez-Delgado et al. (2008). We do not confirm the presence of a second loop. Furthermore, the panels at right show that the location of the Northeastern section of the stream in our data is consistent with the discovery image but in between the two loops of Martínez-Delgado et al. (2008).

a dynamical model without much fine-tuning. In terms of its spatial extent and stellar mass the stream is similar to the Sagittarius stream (see Sesar et al. 2017). The Milky Way and NGC 5907 are also quite similar, which means that the entire system offers an interesting analog to this accretion event.

We now turn to the most puzzling aspect of our study. The morphology of the stream in our data is a good match to the shallower discovery image of Shang et al. (1998) (see Fig. 5), and also to a meta-analysis of NGC 5907 images by Lang, Hogg, & Scholkopf (2014) and to Subaru imaging (see Laine et al. 2016, and S. Laine, priv. communication). However, it is qualitatively different from that reported by M08. The most striking difference is that we do not confirm the presence of the second loop. In fact, the leading tail in the Dragonfly image falls *in between* the two loops identified in M08 (right panels of Fig. 5). Furthermore, there are several other discrepancies: the extent of the Western stream is greater in our data; the stream has more substructure and brightness variations; and the ratio of the apparent width of the stream to the apparent width of the NGC 5907 disk is much smaller.

We cannot definitively determine the cause of these discrepancies with M08, but a likely explanation lies in the image processing procedures that were applied to the data. The M08 data were obtained and processed by an experienced amateur astronomer. Amateurs have played an important role in this field as they convincingly demonstrated the power of small

telescopes for low surface brightness imaging (see Martínez-Delgado et al. 2010). However, the methods that are used by the amateur community typically do not allow for quantitative analysis, as their image processing is generally optimized for aesthetic qualities rather than preserving the linearity and noise properties of the data.

There are several routes to making further progress. In the current 5 hrs of observation we have not yet reached the point where systematic effects dominate over the Poisson noise, and deeper data can verify the reality of the tentative sections of the stream and better quantify its substructure. We will also search for streams around other galaxies, both in targeted surveys (Merritt et al. 2016; C. Gilhuly et al., in preparation) and in blank field surveys (S. Danieli et al., in preparation). More generally, this study follows previous work in demonstrating the power of the combination of low surface brightness imaging with dynamical modeling (see also, e.g., Foster et al. 2014; Amorisco, Martínez-Delgado, & Schedler 2015; Pearson et al. 2019). Systematic surveys of accretion events across the nearby Universe are within reach, providing complementary information to the extensive work in the Local Group.

We thank the staff at New Mexico Skies for their excellent support, and David Martínez-Delgado for helping us understand aspects of his imaging.

REFERENCES

- Abraham, R. G. & van Dokkum, P. G. 2014, *PASP*, 126, 55
 Amorisco, N. C., Martínez-Delgado, D., & Schedler, J. 2015, arXiv e-prints, arXiv:1504.03697
 Arp, H. 1966, *ApJS*, 14, 1
 Atkinson, A. M., Abraham, R. G., & Ferguson, A. M. N. 2013, *ApJ*, 765, 28
 Bell, E. F., Naab, T., McIntosh, D. H., Somerville, R. S., Caldwell, J. A. R., Barden, M., Wolf, C., Rix, H.-W., et al. 2006, *ApJ*, 640, 241
 Belokurov, V., Evans, N. W., Irwin, M. J., Lynden-Bell, D., Yanny, B., Vidrih, S., Gilmore, G., Seabroke, G., et al. 2007, *ApJ*, 658, 337
 Bertin, E. & Arnouts, S. 1996, *A&AS*, 117, 393
 Bonaca, A., Conroy, C., Price-Whelan, A. M., & Hogg, D. W. 2019, arXiv e-prints, arXiv:1906.02748
 Bonaca, A. & Hogg, D. W. 2018, *ApJ*, 867, 101
 Bovy, J., Erkal, D., & Sanders, J. L. 2017, *MNRAS*, 466, 628
 Bullock, J. S. & Johnston, K. V. 2005, *ApJ*, 635, 931
 Danieli, S., van Dokkum, P., & Conroy, C. 2018, *ApJ*, 856, 69
 Fardal, M. A., Huang, S., & Weinberg, M. D. 2015, *MNRAS*, 452, 301
 Forbes, D. A., Beasley, M. A., Bekki, K., Brodie, J. P., & Strader, J. 2003, *Science*, 301, 1217
 Foster, C., Lux, H., Romanowsky, A. J., Martínez-Delgado, D., Zibetti, S., Arnold, J. A., Brodie, J. P., Ciardullo, R., et al. 2014, *MNRAS*, 442, 3544
 Grillmair, C. J. & Carlin, J. L. 2016, in *Astrophysics and Space Science Library*, Vol. 420, Tidal Streams in the Local Group and Beyond, ed. H. J. Newberg & J. L. Carlin, 87
 Hammer, F., Yang, Y. B., Wang, J. L., Puech, M., Flores, H., & Fouquet, S. 2010, *ApJ*, 725, 542
 Helmi, A. 2004, *ApJ*, 610, L97
 Ibata, R., Irwin, M., Lewis, G., Ferguson, A. M. N., & Tanvir, N. 2001, *Nature*, 412, 49
 Ibata, R. A., Lewis, G. F., Irwin, M. J., & Quinn, T. 2002, *MNRAS*, 332, 915
 Ibata, R. A., Wyse, R. F. G., Gilmore, G., Irwin, M. J., & Suntzeff, N. B. 1997, *AJ*, 113, 634
 Laine, S., Grillmair, C. J., Capak, P., Arendt, R. G., Romanowsky, A. J., Martínez-Delgado, D., Ashby, M. L. N., Davies, J. E., et al. 2016, *AJ*, 152, 72
 Lang, D., Hogg, D. W., & Scholkopf, B. 2014, *JMLR Workshop and Conference Proceedings*, 33, 549 (arXiv:1406.1528)
 Law, D. R. & Majewski, S. R. 2010, *ApJ*, 714, 229
 Malhan, K., Ibata, R. A., & Martin, N. F. 2018, *MNRAS*, 481, 3442
 Malin, D. & Hadley, B. 1997, *PASA*, 14, 52
 Martínez-Delgado, D., Gabany, R. J., Crawford, K., Zibetti, S., Majewski, S. R., Rix, H.-W., Fliri, J., Carballo-Bello, J. A., et al. 2010, *AJ*, 140, 962
 Martínez-Delgado, D., Peñarrubia, J., Gabany, R. J., Trujillo, L., Majewski, S. R., & Pohlen, M. 2008, *ApJ*, 689, 184
 McConnachie, A. W., Huxor, A., Martin, N. F., Irwin, M. J., Chapman, S. C., Fahlman, G., Ferguson, A. M. N., Ibata, R. A., et al. 2008, *ApJ*, 688, 1009
 Merritt, A., van Dokkum, P., Abraham, R., & Zhang, J. 2016, *ApJ*, 830, 62
 Mihos, J. C., Harding, P., Feldmeier, J., & Morrison, H. 2005, *ApJL*, 631, L41
 Moore, B., Ghigna, S., Governato, F., Lake, G., Quinn, T., Stadel, J., & Tozzi, P. 1999, *ApJ*, 524, L19
 Newberg, H. J., Yanny, B., Rockosi, C., Grebel, E. K., Rix, H.-W., Brinkmann, J., Csabai, I., Hennessy, G., et al. 2002, *ApJ*, 569, 245
 Odenkirchen, M., Grebel, E. K., Rockosi, C. M., Dehnen, W., Ibata, R., Rix, H.-W., Stolte, A., Wolf, C., et al. 2001, *ApJ*, 548, L165
 Pearson, S., Starkenburg, T. K., Johnston, K. V., Williams, B. F., & Ibata, R. A. 2019, arXiv e-prints, arXiv:1906.03264
 Price-Whelan, A. M. 2017, *The Journal of Open Source Software*, 2, 388
 Price-Whelan, A. M. & Bonaca, A. 2018, *ApJ*, 863, L20
 Sackett, P. D., Morroni, H. L., Harding, P., & Boroson, T. A. 1994, *Nature*, 370, 441
 Sancisi, R. 1976, *A&A*, 53, 159
 Sasaki, T. 1987, *PASJ*, 39, 849
 Sesar, B., Hermitschek, N., Dierickx, M. I. P., Fardal, M. A., & Rix, H.-W. 2017, *ApJ*, 844, L4
 Shang, Z., Zheng, Z., Brinks, E., Chen, J., Burstein, D., Su, H., Byun, Y.-i., Deng, L., et al. 1998, *ApJ*, 504, L23
 Shipp, N., Drlica-Wagner, A., Balbinot, E., Ferguson, P., Erkal, D., Li, T. S., Bechtol, K., Belokurov, V., et al. 2018, *ApJ*, 862, 114
 Tully, R. B., Courtois, H. M., & Sorce, J. G. 2016, *AJ*, 152, 50
 van Dokkum, P. G. 2005, *AJ*, 130, 2647
 van Dokkum, P. G., Abraham, R., & Merritt, A. 2014, *ApJL*, 782, L24
 Wang, J., Hammer, F., Athanassoula, E., Puech, M., Yang, Y., & Flores, H. 2012, *A&A*, 538, A121
 Zhang, J., Abraham, R., van Dokkum, P., Merritt, A., & Janssens, S. 2018, *ApJ*, 855, 78
 Zheng, Z., Shang, Z., Su, H., Burstein, D., Chen, J., Deng, Z., Byun, Y.-i., Chen, R., et al. 1999, *AJ*, 117, 2757
 Zou, H., Zhang, T., Zhou, Z., Peng, X., Nie, J., Zhou, X., Fan, X., Jiang, L., et al. 2018, *ApJS*, 237, 37